communications earth & environment

ARTICLE

https://doi.org/10.1038/s43247-023-00867-6 OPEN

Valleys are a potential refuge for the Amazon lowland forest in the face of increased risk of drought

Marius J. Pohl[1✉], Lukas W. Lehnert[2], Boris Thies[1], Konstantin Seeger[1], Mónica B. Berdugo[3], S. Robbert Gradstein[4], Maaike Y. Bader[3] & Jörg Bendix[1]

The Amazon rainforest is home to an incredible variety of plant and animal species and plays a crucial role in regulating the Earth's climate. Climate change and human activities are putting this important ecosystem at risk. In particular, increasing droughts are making it harder for certain organisms to survive. Here we analyse a satellite-based data set of fog/low-stratus (FLS) frequency and a spatio-temporal drought index. We show that vulnerable organisms may find refuge in river valleys where FLS provides a source of moisture. We find that these favourable microclimates exist throughout the Amazon basin, with the highest occurrence and stability in steep river valleys. We suggest that protecting these hygric climate change refugia could help preserve the biodiversity and functioning of the Amazon ecosystem in the face of future droughts. This would also help stabilise atmospheric moisture recycling, making the region more resilient to climate change.

[1] University of Marburg, Department of Geography, Laboratory for Climatology and Remote Sensing, Deutschhausstraße 12, 35032 Marburg, Germany. [2] Department of Geography, Ludwig-Maximilians-Universität, Luisenstr. 37, 80333 Munich, Germany. [3] University of Marburg, Department of Geography, Ecological Plant Geography, Deutschhausstraße 10, 35032 Marburg, Germany. [4] Meise Botanic Garden, 1860 Meise, Belgium. ✉email: marius.pohl@geo.uni-marburg.de

The Amazon Basin comprises the largest contiguous tropical rainforest on Earth. This region harbours a large number of species[1,2] and provides countless ecosystem services such as climate regulation[3,4]. The Amazon lowland forest is also an important long-term carbon sink[5–7] that can help mitigate global climate-change. However, climate and land use changes are threatening the biodiversity, ecosystem functions and, particularly, climate regulation abilities of this rainforest[4,5]. The Amazon is still suffering from very high deforestation rates[8] and even more from the adverse effects of forest degradation by selective logging[9]. At the same time, climate change is leading to warming temperatures and larger-scale droughts in the Amazon basin[10]. Severe droughts occurred in 2005 and 2010; these droughts were related to positive sea surface temperature (SST) anomalies in the northern tropical Atlantic. Negative rainfall anomalies were mainly observed in south-western Amazonia in 2005 and in south-western Amazonia, Mato Grosso and Bolivia in 2010 while the north-western (NW) area experienced positive rainfall anomalies[11,12]. During the severe 2015/16 drought caused by the El Niño phenomenon, negative rainfall anomalies occurred all over Amazonia, and the drought strength increased towards the eastern Amazon basin. The warming rates exceeded those of previous major El Niño events (e.g. 1982/83 and 1997/98)[13–15]. In addition to this general tendency towards longer and more intense drought conditions[16], future projections conducted for the Amazon Basin have shown either an intensification of drought conditions, with negative rainfall anomalies in the central and eastern Amazon[17], or drought hotspots in the south-central Amazon in June-July-August (JJA)[18]. Positive feedback loops between large-scale deforestation and rainfall reductions[19] are predicted to even exacerbate the future drought situation[13]. As a result, scientists have expressed major concern that the Amazon region is close to a severe tipping point[20] in which the westward transport of moisture from the Atlantic will be inhibited by the increasing reduction in evapotranspiration-driven water recycling[20,21]. This inhibition would endanger not only the carbon sink function[2,10] of the Amazon but also its biodiversity[22].

The most threatened species are those that directly depend on atmospheric moisture and rainwater such as epiphytic communities in the forest canopy. In general, global forest canopies host ~40% of all existing species and are among the most species-rich habitats[23]. Canopy epiphytes serve important ecosystem functions such as intercepting rain-water, sequestering carbon and regulating greenhouse gases. These epiphytes further provide habitats and food resources for organisms at higher trophic levels such as canopy ant communities[24–27]. Tropical montane cloud forests (TMCF) as well as tropical lowland cloud forests (TLCF) are characterised by both high species richness and high abundances of epiphytes. Both of the forest types receive water supply through cloud immersion. The difference between the two forest types is that advection of clouds leads to water inputs in TMCF, while in areas covered by TLCF longwave radiation and generated katabatic flows result in the formation of fog and low-stratus clouds (FLS)[28–30]. The difference between TLCF and tropical lowland rainforests (TLRF) is that the latter do not experience occult precipitation from FLS. This reduces water availability within the canopy and leads to a reduced radiation shelter both contributing to a reduced epiphyte biodiversity[31]. A good example for TLCF is an area previously studied in French Guiana[28,31–33]. However, the spatial distribution of this hygric habitat type is unknown to date, though these habitats may provide hygric climate change refugia (HCCR) in the Amazon basin if the favourable microclimate conditions can persist under the projected intensified drought conditions. In general, HCCR provide stable microclimatic conditions under macroclimatic changes such as warming or variable atmospheric moisture supply. These refugia warrant the survival of species that are poorly adapted to the increasingly adverse atmospheric conditions on the macroscale[34–37].

Buffering warming has thus far been thought to be the most desired property of climate-change refugia. However, for moisture-dependent organisms, HCCR are needed to provide an additional buffer against increasing water scarcity[38]. For many canopy species, regular water inputs in the form of rain or occult precipitation from FLS and dew provide optimal conditions. For non-vascular epiphytes (mosses, liverworts and lichens), it is additionally important how these inputs are timed relative to the timing of light availability, as moisture is quickly lost from these organisms as air dries. FLS can increase the amount of water input to epiphytes and reduce evapotranspiration losses[38] by providing a low-radiation, relatively cool and humid environment. Such conditions can be found in TLCF canopies, where relatively high air humidity, reduced morning radiation stress and wetted plant surfaces by FLS water have been observed[28]. Here, we hypothesise that mainly concave landforms may provide conditions similar to TLCFs over the entire Amazon lowland rainforest and may serve as potential HCCR under drought conditions (Fig. 1a). FLS is expected to preferentially emerge in these landform regions due to the relatively weak atmospheric mixing, increased humidity and low evapotranspiration losses[28,38]. Furthermore, the nocturnal katabatic flows not only facilitate the formation of FLS but also contribute to the reduction of temperature in valleys, thereby locally mitigating effects of global warming[39]. However, to date, it is largely unknown to what extent TLCF conditions persist under regional droughts and how these potential HCCR are spatially distributed. This knowledge is urgently needed to prioritise protection measures under climate change.

Therefore, the main objective of this study is to utilise novel area-wide FLS data[40] to examine the occurrence and resistance of HCCR to past droughts which could mimic future conditions in the Amazon due to climate change. In detail, we analysed 18 years of data representing FLS occurrence over the Amazon basin[40] in four sectors (NW, NE, SW and SE). The sectors have been delineated from the drought anomaly patterns of the major Amazon droughts of the past decades[15]. We specifically investigated FLS frequencies (Fig. 1c) in these sectors, paying particular attention to the terrain and regional drought conditions, in order to understand the persistence of TLCF under varying climatic boundary conditions and identify potential HCCR.

Results

FLS occurrence and TLCF conditions in the Amazon lowland forest. We found that FLS is a common feature over the entire Amazonian lowland forest under normal conditions (Fig. 1c). Approximately 30% of the entire study area exhibits long-term FLS frequencies that are comparable to those found in the locations of French Guiana where TLCF is known to occur. Furthermore, about 15% of the study area has an even higher long-term average FLS frequency of ~50%. The annual FLS frequencies are generally higher in concave landforms than in other landforms and are higher during the rainy season than in the dry season (Fig. 1a, Supplementary Figs. 1, 2) over all sectors (Supplementary Fig. 2). There is an E-W FLS gradient, with higher frequencies in the east, which we suggest to result from the Atlantic moisture advection being reduced towards the western parts (Supplementary Fig. 2). This is supported by the relatively high specific air humidity particularly in the NE sector, which may foster FLS formation (Supplementary Fig. 3). Interestingly, the relatively strong rainfall seasonality in the west (Supplementary Fig. 2) is only weakly reflected in the seasonal patterns of FLS

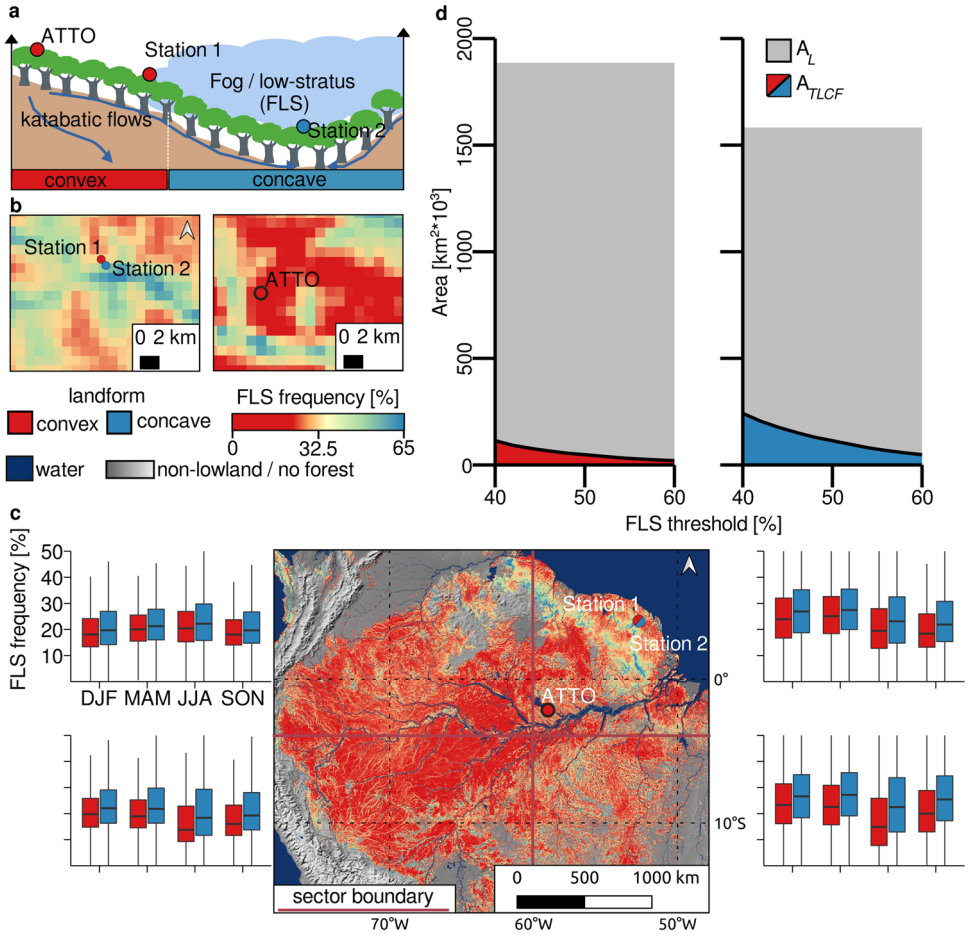

Fig. 1 FLS formation mechanism, frequencies and TLCF conditions measured in different landform types and sectors of the Amazon Basin. a Idealised cross section illustrating at which topographic position the threshold between TLCF and non-TLCF conditions is expected to be reached. This figure is intended to familiarise the reader with the mechanism of FLS formation in concave terrain of TLCF (for a process-based modelling analysis of this assumption, see S3). **b** Subset of the FLS frequencies of the three sites used to determine typical FLS thresholds corresponding to TLCF conditions (≥40% FLS). **c** FLS frequency map (2003–2020) indicating the location of three typical sites with convex (Amazon Tall Tower Observatory ATTO; 13% long-term FLS-frequency) and Station 1; 32% long-term FLS-frequency) and concave (Station 2; 50% long-term FLS-frequency) landforms, shown in **1b**, that have undergone canopy epiphyte analyses and thus, TLCF condition analyses[28,32,33,39,42]. Boxplots depict the seasonal FLS frequency per sector and landform (median and upper/lower quartiles). **d** Total area of FLS frequencies meeting potential TLCF conditions depending on landform type. A_L is the total area of concave and convex landforms in the study domain (grey areas), A_{TLCF} is the area with suitable conditions for TLCF, defined by different FLS frequency thresholds (*x*-axis).

frequencies, which is quite low over the entire Amazon region (Fig. 1c). The NW sector exhibits a great seasonal stability in FLS occurrence; this can be related to the annually stable low saturation deficit in this region (Supplementary Fig. 3). In contrast to the NW sector, where close-to-saturation conditions presumably lead to only small differences in FLS frequencies among landform types (Supplementary Fig. 3), we show for all other sectors that FLS conditions are relatively stable throughout the year in concave landforms. At the same time, we observed a clear decrease in the FLS frequency towards the relatively dry months in convex landforms; this finding is particularly prominent in the SE sector (Fig. 1c).

To determine the FLS range corresponding to potential TLCF conditions, we extracted the FLS frequencies at sites with and without proven TLCF conditions. We revealed that TLCF conditions persist in the Pararé River valleys (concave landforms) where an annual FLS frequency of 40% was found (Fig. 1b, *Station 2*)[31,33,41]. We recognised the transition to non-TLCF conditions[41] at an FLS threshold below 40% (Fig. 1b, Station 1). Another recent study revealed clear non-TLCF conditions with scarce epiphyte occurrences at very low FLS frequencies in a convex landform situation (Fig. 1b, Amazon Tall Tower Observatory, ATTO)[42]. Because no exact FLS threshold corresponding to TLCF conditions is known, we analysed the FLS frequency range of 40–60% as potential HCCR. We can show that the conditions required for such HCCR are more frequently found in concave landscapes than in convex landscapes, but convex landforms compose the dominant portion of the Amazon Basin (see Fig. 1d, A_L). Increasing the FLS threshold beyond 40% reduces the potential refugial area nonlinearly in both landform types but results in a clearly higher remaining area in concave terrain than in convex terrain (Fig. 1d).

Potential HCCR area per sector and landform type. We found a higher proportion of concave landforms than convex landforms that could be considered HCCR in all four sectors (Fig. 2). However, some convex landforms are also found to be suitable as refugial areas in all sectors. We detect the lowest proportions of these landforms in the SE sector (Fig. 2c). We further showed that the available refugial area decreases nonlinearly with an increasing FLS threshold in all sectors. The NW sector is characterised

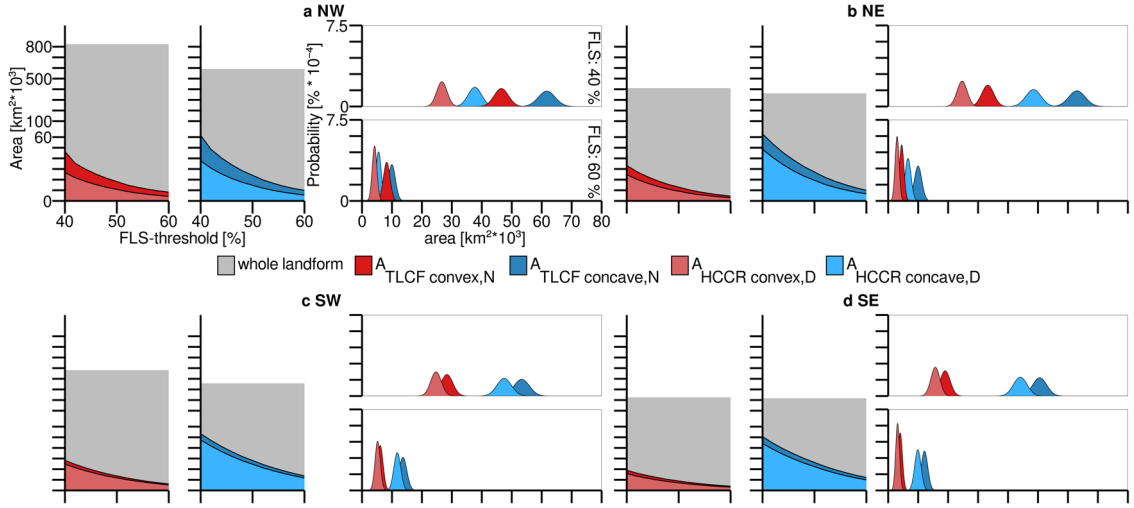

Fig. 2 Total area providing HCCR conditions within each landform type depending on the established FLS frequency threshold. a NW **b** NE **c** SW **d** SE sectors of the Amazon Basin under normal conditions ($A_{TLCF\ convex,N}$, $A_{TLCF\ concave,N}$; dark-red and dark-blue areas, all grid-cells with SPEI ≥ −0.5) and drought conditions with SPEI ≤ −0.5 ($A_{HCCR\ convex,D}$, $A_{HCCR\ concave,D}$; light-red and light-blue areas). Please note that the scale of the *y*-axis changes at 60*10³ km². From the value 100*10³ km² the axis is compressed by the factor 10. Density distributions represent Monte Carlo Simulations (Methods Section) derived samples of TLCF (dark-red and dark-blue) and HCCR (light-red and light-blue) areas per landform at FLS-thresholds of 40 and 60%. The HCCR area is the area within each sector where the FLS frequency under drought conditions remains higher than or equal to the respective FLS frequency threshold value shown on the *x*-axis. Potential refugial areas are significantly ($p < 0.001$) larger in concave landform regions than in convex-landform regions in all sectors and for all FLS frequency thresholds under both normal and drought conditions. The differences in TLCF/ HCCR areas between normal and drought conditions decrease with increasing FLS threshold.

by the strongest decrease in concave landforms. Here, the concave HCCR area is ~9500 km² smaller than the corresponding TLCF area. Thus, this sector shows the lowest stability (Fig. 2a). The southern sectors show the smallest decreases for concave landforms. Here, the concave HCCR area is ~3800 km² smaller than the corresponding TLCF area, but theTLCF areas begin at a lower amount at the 40% FLS frequency level (Fig. 2c, d). In the NE sector, the concave HCCR area is ~8000 km² smaller than the corresponding TLCF area. The convex HCCR area is ~4000 km² smaller than the convex TLCF area. The sector is characterised by a lower decrease in refugial area corresponding to both landforms compared to the NW sector. Here, the concave HCCR area is ~11,000 km² smaller than the corresponding TLCF area. The convex HCCR is ~9000 km² smaller than the convex TLCF area. The NE sector is more influenced by strong moisture advection from the Atlantic resulting in higher specific humidity conditions (Supplementary Fig. 3).

Losses of HCCR under drought conditions. Due to the intensification of drought conditions caused by climate change, moisture-dependent canopy species in the Amazon lowland are highly threatened, as noted by[43] and[22]. We used all grid cells that exhibit past drought conditions during the study period as a proxy for future droughts. The definition of droughts is based on the Standardised Precipitation Evapotranspiration Index (SPEI)[44,45] where widely used thresholds define drought intensity[46]. According to the calculation of the SPEI product, SPEI drought conditions represent larger-scale meteorologically driven spatial patterns characterised by negative rainfall anomalies combined with high evapotranspiration losses[44,45]. We first showed that the duration of drought conditions decreases with increasing drought intensity by analysing four drought severity classes based on the SPEI (S2, Supplementary Fig. 4). While the findings are consistent over all sectors of the Amazon lowland forest, the SW sector shows the lowest number of drought months occurring during droughts of light and moderate intensities. At the same time, we observed the lowest numbers of extreme droughts in the NW and SW sectors. This finding reflects that the western sector of the Amazon lowland is less affected by strong El Niño-type droughts than the other sectors[14,15]. We then compared the effect of droughts on the potential HCCR conditions per sector for both landform types (*see the Methods section*) and found a general loss of refugial area over all sectors and landforms under drought conditions (Fig. 2). We showed that concave landforms can conserve more refugial areas under drought conditions, while hardly any suitable area remains in convex landforms at very high FLS thresholds (e.g. 60%, Fig. 1). We observe a significantly stronger effect of drought in the northern sectors for both landform types (Fig. 2, Table 1). We found the largest effect, and thus the least stability, in the NW sector (Fig. 2a). The southern sectors do not show any large effect of additional drought conditions. We found that the overall drought influence is significantly stronger when the FLS threshold is low (Table 1). We assume that the few refugial areas remaining under high FLS thresholds are so extraordinarily moist that even droughts do not considerably limit the suitable local FLS condensation conditions. We suggest that the relatively poor moisture supply available in the southern sectors (Supplementary Fig. 3g, h) under the current low drought frequency (Supplementary Fig. 4c, d) results in nearly stable refugial areas at all FLS thresholds.

Because it is expected that droughts in the Amazon Basin will increase in both frequency and intensity for the future[13,16,17], we additionally question which potential HCCR areas have remained stable under past strong-intensity droughts (Fig. 3). We showed that under the lowest FLS threshold (40%) and intensive drought conditions (SPEI < −1.5), the refugial areas associated with concave landforms remain larger than those associated with convex landforms. Between the two most severe drought classes, we find that the greatest areal losses occur in the eastern sectors, particularly among concave landforms (Fig. 3b, d). In these sectors, El Niño-type droughts are the most intense[11,15]. The refugia in the western sectors remain almost stable regardless of the local landform class (Fig. 3a, c).

Table 1 Statistical results derived from virtual samples calculated by a Monte Carlo Simulation ($n = 10\%$ grid-cells per landform per sector, iterations = 500).

Sector	$TLCF_{concave} \geq TLCF_{convex}$		$HCCR_{concave} \geq HCCR_{convex}$		$TLCF_{convex} \geq HCCR_{convex}$		$TLCF_{concave} \geq HCCR_{concave}$	
	FLS: 40%	FLS: 60%	FLS: 40%	FLS: 60%	FLS: 40%	FLS: 60%	FLS: 40%	FLS: 60%
NW	15,170	1700	11,000	1330	19,840	4045	24,000	4430
NE	29,800	5320	23,800	3540	8575	1490	14,530	3270
SW	30,000	7600	22,700	6600	3645	860	5860	1895
SE	29,500	8100	26,500	6800	3090	865	6090	2220

All tests driven are one-sided paired-*t*-tests for differences in TLCF and HCCR areas between landforms ($TLCF_{concave} > TLCF_{convex}$, $HCCR_{concave} > HCCR_{convex}$) and between normal and drought conditions per landform ($TLCF_{concave} > HCCR_{concave}$, $TLCF_{convex} > HCCR_{convex}$). The mean differences (D in km^2) between the tested groups are presented. We applied one-sided paired-*t*-tests for the comparison of Monte Carlo Simulation derived means of TLCF and HCCR within each landform and one-sided unpaired-*t*-tests for the comparison of means of TLCF and HCCR between both landforms. The reported area differences are highly significantly different from 0 ($p < 0.001$).

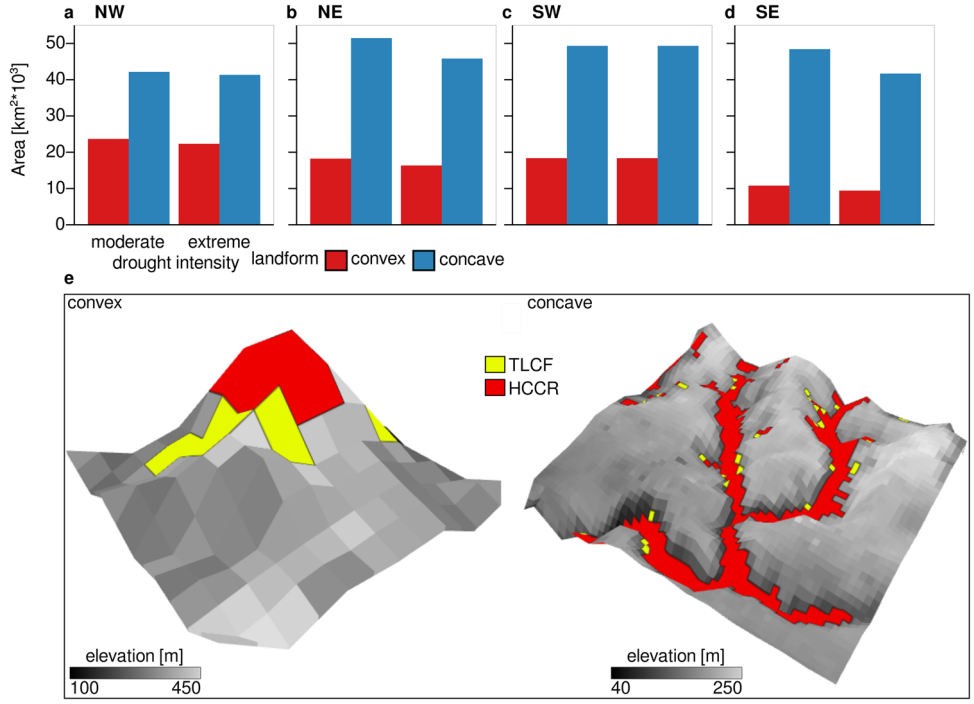

Fig. 3 Potential HCCR areas and examples of TLCF and HCCR in convex and concave landforms under normal and intensive drought conditions. **a**–**d** Potential HCCR areas in different sectors derived using an FLS threshold of 40% under intensive drought conditions per landform class and sector). **e** TLCF and HCCR areas in western Surinam (4.62° N, 56.78° W, convex) and Brazil, east to Santa Rosa (2.93° S, 53.35° W, concave). Only the upper part of the local mound remains stable as HCCR under normal and intensive drought conditions in the convex landform shape. The mean elevation of the convex HCCR differs comparatively strongly from that of the convex TLCF (difference is +22). The HCCR are located on average 22 metres higher than the TLCF in the same area. The TLCF is spreading throughout the concave valleys. The HCCR are located slightly further towards the centre of the valley compared to the TLCF whereas steep valley slopes and valley centres remain stable. The mean elevation of the concave HCCR differs very slightly from that of the concave TLCF (difference is −1). On average the HCCR are located at almost the same elevation and therefore topographic position in the concave valley as the TLCF.

We further analysed the development of the topographic position index (TPI) under intensive drought conditions and different FLS thresholds to understand the role of the terrain configuration in affecting the stability of HCCR. We found that the remaining areas show an increasing steepness associated with both landform types (compare Fig. 3e, f). In convex terrain, only high elevation areas remain HCCR under severe droughts (Fig. 3e). Under intensive droughts, FLS is concentrating in the valley centre while the higher slopes become FLS-free and thus, do not belong anymore to the HCCR (Fig. 3f).

Loss of potential TLCF areas according to modelled deforestation scenarios in the Amazon basin. The ongoing deforestation threatens the TLCF areas and thus the HCCR. This also directly threatens the habitats of tree canopy epiphytes. To test the spatial impact of deforestation, we compared the potential TLCF areas (FLS frequency ≥40%) to two different deforestation scenario models[47] in 2050 (method section, S4, Supplementary Fig. 6). Deforestation rates according to the Governance-Scenario would result in loss rates of about 9% of the potential TLCF area on average across all sectors. Deforestation rates as in the Business-As-Usual-Scenario would result in substantially higher loss rates that vary across the sectors. The lowest exposure to modelled deforestation and thus, loss of potential TLCF area is expected for the NW sector. The SW sector is much more vulnerable and could lose up to one-third of its potential TLCF area. The eastern sectors would be at much higher risk and could lose about half of the potential TLCF area (Table 2).

Table 2 Deforestation models[47] and derived impact on potential TLCF/HCCR area.

Sector	Model/year	Remaining TLCF [km²]	Loss compared to GOV 2020 [%]
NW	GOV 2020	89,041	---
NE	GOV 2020	92,610	---
SW	GOV 2020	71,228	---
SE	GOV 2020	59,688	---
NW	GOV 2050	84,442	5
NE	GOV 2050	83,331	10
SW	GOV 2050	62,708	12
SE	GOV 2050	54,503	9
NW	BAU 2050	78,098	12
NE	BAU 2050	48,293	48
SW	BAU 2050	46,796	34
SE	BAU 2050	26,109	56

Remaining area of TLCF for FLS-frequency > 40% before and under indicated future deforestation scenarios.
GOV Governance-Model, *BAU* Business-As-Usual-Model.

Discussion

In this work, we used past drought conditions in the Amazon basin as a surrogate to examine the potential future climate. We found that FLS and, thus, HCCR conditions exist all over the Amazon lowland forest. However, we demonstrated a clear decrease in the FLS frequency during the dry season in the different sectors of the Amazon basin. Relatively low FLS frequencies occur in the southern sector due to its longer dry season, resulting in lower relative HCCR proportions, especially those associated with convex-shaped topography. We found a general decrease in high-FLS areas among all sectors and landform types under past drought conditions. However, concave landforms showed by far the highest persistence of FLS, thus providing favourable microclimatic conditions under regional droughts. We identified concave landforms in the Amazon lowland as stable HCCR given a drought-prone future climate in the region. However, not all concave terrain areas exhibit high resistance under dry conditions. This is because the shape of the terrain serves only as a general indicator of local hydrological HCCR conditions and thus, its use is limited. Local water availability and atmospheric humidity are important for FLS formation. In addition, valley slopes and convex surroundings must be of sufficient steepness and size to allow for cold air production and the development of nocturnal katabatic flows as in the area of the Inselbergs in French Guiana[28]. Normally, concave terrain can receive soil water and overland flow from adjacent higher terrain, which provides a moisture source necessary for FLS formation, particularly under dry conditions. On the one hand, concave landforms without river courses are less effective atmospheric moisture sources. On the other hand, factors including soil type, depth, and surface roughness can adversely modify cold air, overland, and soil water fluxes and thus hinder FLS formation. All these factors should be considered in future higher-resolution studies on HCCR. We reveal that particularly steep valleys, but also the adjacent convex slopes and slopes at the base of high terrain, can withstand intensive droughts. The reason for this is that nocturnal outgoing radiation losses increase during droughts, thus fostering FLS formation also in the tropics when cold air drainage flows occur in steep terrain[28,48–50] (Supplementary Fig. 5). To support the role of katabatic flows for FLS formations in tropical lowland valleys we compare the FLS occurrence with spatially derived cold air drainage flows using a process-based model (S3). This process is particularly important in the southern and the NE sector of the Amazon basin, where the adverse effects of strong land-use changes on the regional water cycles are most prominent and exacerbate the effects of global climate change[51–53]. However, we also show that past extreme drought conditions were most prominent in the NE sector. This is related to droughts following strong El Niño events, which are projected to become even longer and more intense under future climate change[43,54].

It is of interest how the shelter effect of concave topography against local drying during meteorological droughts is linked to the current debate on Amazon forest dieback mechanisms under combined climate and land use changes. The starting point for forest dieback occurs at a certain level of drying, which corresponds to a reduction of ~3 mm of rainfall per day[54]. The importance of a closed canopy in the western Amazon due to the increasing fraction of rainwater recycling by the forest was emphasised by[5]. Only trees can access water from deeper soil layers during drought conditions, preventing drought stress and fire risks in the understory. The importance of maintaining the structure of natural forests to reduce self-amplified forest dieback under increasing meteorological droughts was underscored by[55].

Moisture-dependent ecosystems are highly threatened by droughts, enhanced fires[55] and forest degradation[56] reducing atmospheric moisture. High resistance of HCCR during intensive droughts under sheltering concave terrain conditions will not directly buffer negative rainfall anomalies because the amount of occult precipitation from FLS at canopy level is likely too low to directly supply rainforest trees. However, there are indirect effects to consider. For instance, the reduction of radiation stress by FLS can buffer desiccation and even the risk for fire[5]. Therefore, persistent HCCR conditions in concave terrain could delay forest dieback, especially in the case of open canopies at the deforestation front, which are particularly vulnerable to increasing meteorological drought conditions[5,55]. Buffering desiccation in the understory is particularly crucial when the tipping point for self-amplified forest dieback in combination with grass invasion is reached under future climate conditions[5]. At the same time, the tipping point for a critical reduction of rainfall with regard to forest dieback is at around 30–50% deforestation of the Amazon forests[57]. Nocturnal and early morning canopy wetting by FLS in HCCR under intensive droughts might help to shift this tipping point towards enlarged deforestation areas by providing higher canopy ET during the day which can foster local rainfall formation. Rainfall formation in the western part of the Amazon is more and more depending on the recycled vapour through ET instead of rainfall directly formed from the Atlantic moisture advection as in the easternmost parts of the Amazon. Thus, the highest dependence of rainfall on ET is found in the far western sectors near the Andes[58]. Generally, FLS-moistened canopies can enhance moisture support and sustain aerial rivers and lakes[58,59]. Under arid conditions, the persistence of FLS in concave terrain is relatively high in the western sectors, indicating that these areas likely foster the regional resilience of the forest. In this regard, higher evapotranspiration in FLS-driven HCCR especially close to the deforestation front would contribute to the resistance of the Amazon forest against environmental changes. Based on our results we highly recommend protecting the HCCR, particularly in these vulnerable sectors. We finally suggest that areas with HCCR conditions should be priority areas of conservation, especially in the eastern part of the Amazon basin. In contrast to this urgent suggestion, these areas in the Amazon lowland forest have, to date, been primarily subject to multiple land use conflicts.

Since World War II, development policies for the Amazon have focused on fostering private colonisation programs instead of agrarian reforms in already settled areas[60]. This led to high deforestation and forest degradation rates, only interrupted by a period of deforestation control and sustainable development

(~2004–2012[61]), followed by dismantling environment laws and a lack of environmental governance[62]. Particularly riverine, and thus, major HCCR areas, were and are heavily affected by dam constructions, illegal mining and often are the starting point for deforestation[61,63,64].

Among the focal areas of recent infrastructure programmes, further intensification is planned, including new dam[65] projects. Thus, the effects of conserving concave-shaped HCCR areas might go far beyond safeguarding the diversity of moisture-dependent organisms in lowland forest canopies under climate change. First, protecting these areas would help other specialised and endemic organisms cope with climate change[66]. Second, comprehensive action could also help to prevent adverse effects on river-sediment transport, aquatic biodiversity, greenhouse mitigation and river connectivity[67]. Third, conservation would help to protect the riparian systems of the Amazon lowland, as these systems are fundamental for providing key ecosystem-regulating services[68]. Finally, it has been shown that reducing deforestation in areas close to human settlements, such as river valleys, through protection can have far-ranging influences on the resilience of the Amazon lowland forests over quite large spatial scales beyond the areas of refugial valleys[10].

It must also be stressed, that riverine areas are heritage sites of great historical value, harbouring most of the archaeological sites and historical settlements of Amazon indigenous people[69]. While indigenous people are mainly threatened by activities such as land grabbing and illegal mining[70] they at the same time have the highest knowledge on locally adapted and sustainable land use practices including agroforestry. Empowering their abilities would therefore be the most effective approaches to forest conservation in riverine areas[71,72], thus also safeguarding HCCR. As a consequence, protecting HCCR might have value beyond conservation of biodiversity and stabilising the local hydrological cycle under droughts. Thus, we suggest embedding HCCR protection in a broader governance concept, following a landscape approach considering HCCR and adjacent areas[61]. Protecting HCCR areas should be aligned with the support of indigenous people and their sustainable agroforestry management, including forest restoration measures in deforested or degraded areas with special reference to maintenance of HCCR functionality. This, however, can only be achieved through a close cooperation of several actor groups: indigenous people, smallholders, the agrobusiness, and local to national governments[61].

Methods

Study area. We focus our study on the region of the Amazon lowland forest with elevations ≤500 m above sea level (asl) (Supplementary Fig. 7). This area has been shown to harbour tropical lowland cloud forest (TLCF) ecosystems which are candidates for HCCR, particularly for drought-sensitive canopy organisms[28,39,73]. The prerequisites that were needed for a region to be included in this study were that (1) the area must be below 500 m a.s.l. according to the Advanced Spaceborne Thermal Emission and Reflection Radiometer global digital elevation map (ASTER GDEM)[74] and (2) must harbour long-term pristine lowland forest areas. For the latter, the Food and Agriculture Organization (FAO) Land Cover Classification System (LCCS1)[75] was used to define forested areas, and the Moderate-resolution Imaging Spectroradiometer (MODIS) land cover product (MCD12Q1)[76,77] was incorporated. For the analysis, only grid cells classified as evergreen broadleaf forest in 2019 and for at least 10 contiguous years previously were considered.

We delineated long-term undisturbed evergreen tropical lowland forest areas based on the FAO LCCS1 and the MCD12Q1 (2001–2019)[76,77]. First, we aggregated the forest cover dataset at a 30 m spatial resolution to the 1 km spatial resolution of MODIS. This was conducted using a pixel-weighted resolution reduction process. Then, we classified pixels with tree crown coverages ≥60% as tropical evergreen broadleaf forests. Finally, we tested for long-term persistence by using the MCD12Q1 time series (2001–2019)[76,77] and retained only pixels in our study area with at least 10 years of forest cover (**a**). Areas thus identified as long-term forests were filtered to obtain regions with elevations ≤500 m asl using the 1 km resampled ASTER GDEM[74] (**b**). The combination of (**a**) and (**b**) yielded the object of investigation: regions in which the conditions implicate potential TLCF, serving as a surrogate of HCCR, where supported by atmospheric conditions (**c**). This process reduced the evaluated area to 3,443,845 km². We also subdivided the Amazon area into four sectors (NE, NW, SE, and SW) based on the contrasting spatial patterns of recent Amazon droughts (Fig. 1)[17].

Derivation of landforms. Landforms are expected to be an important driver of FLS development in the Amazon basin[28]. In this article, we therefore considered two main types of landform classes: (1) convex-shaped and (2) concave-shaped landforms. Information on these landforms was derived from a digital elevation map (DEM) by calculating the topographic position index (TPI)[78]. For this purpose, we calculated the relative height of each grid cell within its 7-by-7 neighbourhood. Negative values describe cells that are lower than the mean elevation of the neighbouring pixels (indicating a concave landform shape), while positive values consequently describe pixels that are higher than their neighbouring grid cells (indicating a convex landform shape) (Supplementary Fig. 8). At a constant pixel resolution, a relatively high TPI indicates a greater height difference and thus a higher landform steepness (Fig. 3f). We assumed that pixels with TPI values equal to or larger than zero represented plain or elevated areas and thus classified them as convex landforms (1). Grid cells with negative TPI values were classified as concave landforms.

$$\text{convex} = \text{TPI} \geq 0 \quad (1)$$

$$\text{concave} = \text{TPI} < 0 \quad (2)$$

The amplitude of the TPI values is particularly important, as strongly negative TPI values account for steep valleys and valley centres (local minima), while highly positive TPI values account for steep terrain rises and high elevations (local maxima).

FLS and meteorological datasets. The study was based on a new comprehensive FLS occurrence dataset constructed over the Amazon basin from night-time satellite images acquired by the Aqua MODIS platform[39,40]. Aqua MODIS overflights conducted over the South American continent provide thermal infrared imagery between 2 and 6 a.m. local time; these imagery were used to spatially derive daily composites of nocturnal radiation associated with FLS[39,40] for the entire study area. Based on reference cloud-free MODIS scenes and a spatially dynamic threshold derived while considering the potential subpixel FLS coverage, FLS pixels were identified using brightness temperature differences ΔBT10.8 µm–3.9 µm[40]. The derived daily FLS detection composites were subsequently aggregated to quarterly and total FLS frequencies (Fig. 1). We further used the European Centre for Medium-range Weather Forecasts (ECMWF) Reanalysis version 5-Land (ERA5-Land)[79] data to analyse how relatively large-scale atmospheric conditions may influence FLS conditions in different sectors. FLS mainly occurs during the night and early morning hours (hours 23–8) as a result of radiation processes and katabatic winds. We thus used hourly ERA5-Land data characterising specific and relative humidity for this timespan. To assess rainfall, wind speed and wind direction daily totals were additionally considered. We further aggregated our results to four sectors in the Amazon (Fig. 1) that might adversely impact FLS occurrence and thus hygric refugia resistance against climate change. We aggregated the precipitation data from ERA5-land to mean-monthly quarterly precipitation sums (December-January-February (DJF), March-April-May (MAM), JJA, and September-October-November (SON)) and divided the results according to the NW, NE, SW, and SE sectors (Fig. 1) to identify the relationship between precipitation, wind direction or wind speed and the FLS frequency (Fig. 1). We also calculated the mean relative and specific humidity on a quarterly basis in each sector to identify the varying condensation conditions that most likely affect the FLS frequency.

Seasonal FLS occurrence. We analysed the seasonal FLS frequencies to understand the spatiotemporal dynamics in the Amazon (Fig. 1). This was necessary because the study area spans two hemispheres and experiences various seasonal courses comprising rainy and dry periods with an east–west moisture gradient. We compared the sectoral (NW, NE, SW, and SE) FLS frequencies in different topographic positions with the seasonal wind field and atmospheric humidity conditions to separate climatological and terrain-induced spatial patterns throughout the year. We superimposed the average wind field onto the FLS frequency maps to understand the role of advection processes originating from meso- to larger-scale circulations and their interactions with topography with regards to the spatial FLS pattern (Supplementary Fig. 3).

Detection and classification of droughts. We analysed FLS frequencies under normal conditions and drought conditions. For this purpose, we used the Standardised Precipitation Evapotranspiration Index (SPEI) and considered only pixels where normal and divergent drought conditions occurred during the study period (2003–2018). To detect long-term drought effects, drought and non-drought conditions were separated based on the monthly SPEI grids. We use two different classification schemes. In the first classification scheme, droughts were divided from non-droughts. In the second classification scheme, only moderate and extreme drought conditions were considered[80] (Supplementary Table 1).

The drought classification schemes provided us with a monthly time series of spatially explicit drought occurrences between 2003 and 2018.

Because no single FLS threshold was supported by the FLS conditions at the sites with known TLCF/HCCR occurrences, we applied a further analysis by considering the continuum between FLS frequencies of 40 and 60%. This analysis consisted of 3 steps:

1. Calculation of a landform-dependent TLCF/HCCR occurrence;
2. Sectoral calculation of a landform-dependent HCCR occurrence; and
3. Identification of a drought-dependent HCCR occurrence.

The three steps are described in the following text.

Calculation of a landform-dependent TLCF/HCCR occurrence. To account for the landform-dependent occurrence of TLCF/HCCR conditions, we partitioned the grid cells according to the landform classification. This allowed us to derive the absolute HCCR area in relation to the FLS frequency within each landform and sector as $A_{TLCF/HCCR}$ (FLS).

Drought-dependent HCCR occurrence. In the first step, all pixels were identified for each landform, thus providing HCCR conditions under non-drought conditions corresponding to the respective FLS threshold ($A^{HHCR,N}$ (FLS)). In the second step, drought classes were additionally considered. For each drought class, the corresponding pixels identified in step 1 were extracted, thus still providing HCCR conditions under drought $A^{HCCR,D}$ (FLS).

Calculation of the landform-dependent HCCR occurrence. To account for landform-dependent occurrence HCCR conditions, we partition the grid cells according to the landform classification. This allows us to derive the relative proportion of HCCR in relation to FLS frequencies within each landform considering the following equation:

$$P^{HCCR}{}_{L} = A^{HCCR}{}_{L}(FLS)/A_{L} \quad (3)$$

with:

$P^{HCCR}{}_{L,S}$ is the relative proportion of HCCR in the landform area per sector S, A^{HCCR} is the area with HCCR conditions in landform class L[km²] in relation to the FLS threshold, A_L is the area of landform class L [km²].

Drought-dependent HCCR occurrence. In the first step, all grid-cells are identified for each landform, which provides TLCF conditions under non-drought conditions for the respective FLS threshold ($A^{TN}{}_{L}$(FLS)). In a second step, drought classes are considered. For each drought class, those pixels of step 1 are extracted, which still provide TLCF conditions under drought conditions $A^{TD}{}_{L,S}$(FLS). Mathematically, the approach can be denoted:

$$PR^{HCCR}{}_{L}(FLS) = A^{HCCRD}{}_{L},(FLS)/A^{HCCRN}{}_{L}(FLS) \quad (4)$$

with:

$PR^{HCCR}{}_{L}$(FLS) is the area of drought resistant HCCR in the landform area according to the FLS threshold, $A^{HCCRD}{}_{L}$ (FLS) is the hygric refugial area under drought conditions in the landform class L [km²], $A^{HCCRN}{}_{L}$ (FLS) is the HCCR area under non-drought conditions in the landform class L [km²].

Monte Carlo simulation. To test the robustness of observed differences between regions, FLS thresholds and drought conditions, we applied Monte Carlo Simulations for convex and concave landforms (Supplementary Fig. 9). For the FLS-thresholds at 40 and 60%, 10% of grid cells are randomly selected. Then, FLS frequencies are calculated under normal and drought conditions. By repeating this 500 times, distributions of FLS frequencies are derived for FLS thresholds, drought conditions and landforms. These were normally distributed (p value of Shapiro–Wilk-Test = 0.9). The number of iterations was set to 500 to obtain an approximate normal distribution. The sample size was set at 10% to reflect a representative sample of the total data set. Afterward, we applied two-sample t-tests to test for significant differences between (i) landforms and (ii) normal vs. drought conditions.

Modelled deforestation. For the Amazon Basin, predictions of different deforestation rates until the year 2050 from the SimAmazonia model are available[47]. These modelled deforestation rates are divided into a Business-As-Usual model and a governance model. In the Business-As-Usual scenario, historical deforestation rates are used and combined with major roadway paving. Based on this, a future projection of the deforested area is calculated. Historical deforestation rates are also considered in the governance scenario. However, this scenario sets a maximum deforestation capacity of 50% per Amazon Basin subregion. In addition, existing and planned conservation regions are considered in this scenario. To derive the impact of deforestation trends derived from the different scenarios on the TLCF/HCCR areas, we first calculated the area of the TLCF (FLS frequency ≥ 40%) in the forested areas according to the governance scenario for the year 2020 in the four described sectors. We then compared the spatial extent of the TLCF area in 2020 to the modelled remaining TLCF area in 2050 using the governance scenario and the Business-As-Usual scenario. Classification as a potential TLCF results from FLS frequency above 40% and identification as a forested grid cell.

Data availability

All FLS data used are publicly available via https://doi.org/10.5678/3f41-cd67, https://doi.org/10.5678/10ak-zg71 and https://doi.org/10.5678/d3t8-1z41. FLS data are available as netcdf files in monthly resolution. The datasets contain two layers. "FLS_sum" is the amount of detected FLS events in a month. "FLS_ref" is the amount of possible FLS detection events in a month. FLS frequency is calculated by the formula FLS_sum/FLS_ref. SPEI data are available via https://digital.csic.es/handle/10261/288226 as netcdf files in monthly resolution.

Code availability

All code used to perform the analysis presented is available upon request from the corresponding author M.J.P. via marius.pohl@geo.uni-marburg.de.

Received: 4 October 2022; Accepted: 26 May 2023;
Published online: 03 June 2023

References

1. Cardoso, D. et al. Amazon plant diversity revealed by a taxonomically verified species list. *Proc. Natl. Acad. Sci.* **114**, 10695–10700 (2017).
2. Yang, Y. et al. Post-drought decline of the Amazon carbon sink. *Nat. Commun.* **9**, 1–9 (2018).
3. Brienen, R. J. et al. Long-term decline of the Amazon carbon sink. *Nature* **519**, 344–348 (2015).
4. Gomes, V. H., Vieira, I. C., Salomão, R. P. & ter Steege, H. Amazonian tree species threatened by deforestation and climate change. *Nat. Clim. Change* **9**, 547–553 (2019).
5. Malhi, Y. et al. Climate change, deforestation, and the fate of the Amazon. *Science* **319**, 169–172 (2008).
6. Strand, J. et al. Spatially explicit valuation of the Brazilian Amazon Forest's Ecosystem Services. *Nat. Sustain.* **1**, 657–664 (2018).
7. Gatti, L. V. et al. Amazonia as a carbon source linked to deforestation and climate change. *Nature* **595**, 388–393 (2021).
8. Silva Junior, C. H. et al. The Brazilian Amazon deforestation rate in 2020 is the greatest of the decade. *Nat. Ecol. Evol.* **5**, 144–145 (2021).
9. Matricardi, E. A. T. et al. Long-term forest degradation surpasses deforestation in the Brazilian Amazon. *Science* **369**, 1378–1382 (2020).
10. Boulton, C. A., Lenton, T. M. & Boers, N. Pronounced loss of Amazon rainforest resilience since the early 2000s. *Nat. Clim. Change* **12**, 271–278 (2022).
11. Ciemer, C. et al. An early-warning indicator for Amazon droughts exclusively based on tropical Atlantic sea surface temperatures. *Environ. Res. Lett.* **15**, 094087 (2020).
12. Lewis, S. L., Brando, P. M., Phillips, O. L., Heijden, G. M. F. & van der Nepstad, D. The 2010 Amazon drought. *Science*, **331**, 554–554 (2011).
13. Davidson, E. A. et al. The Amazon basin in transition. *Nature* **481**, 321–328 (2012).
14. Jiménez-Muñoz, J. C. et al. Record-breaking warming and extreme drought in the Amazon rainforest during the course of El Niño 2015–2016. *Sci. Rep.* **6**, 33130 (2016).
15. Panisset, J. S. et al. Contrasting patterns of the extreme drought episodes of 2005, 2010 and 2015 in the Amazon Basin. *Int. J. Climatol.* **38**, 1096–1104 (2018).
16. Ukkola, A. M., De Kauwe, M. G., Roderick, M. L., Abramowitz, G. & Pitman, A. J. Robust future changes in meteorological drought in CMIP6 projections despite uncertainty in precipitation. *Geophys. Res. Lett.* **47**, e2020GL087820 (2020).
17. Duffy, P. B., Brando, P., Asner, G. P. & Field, C. B. Projections of future meteorological drought and wet periods in the Amazon. *Proc. Natl. Acad. Sci.* **112**, 13172–13177 (2015).
18. Cook, B. I., Smerdon, J. E., Seager, R. & Coats, S. Global warming and 21st century drying. *Clim. Dyn.* **43**, 2607–2627 (2014).
19. Leite-Filho, A. T., Soares-Filho, B. S., Davis, J. L., Abrahão, G. M. & Börner, J. Deforestation reduces rainfall and agricultural revenues in the Brazilian Amazon. *Nat. Commun.* **12**, 1–7 (2021).
20. Lovejoy, T. E. & Nobre, C. Amazon tipping point. *Science Advances* vol. 4 eaat2340 (American Association for the Advancement of Science, 2018).
21. Boers, N., Marwan, N., Barbosa, H. M. & Kurths, J. A deforestation-induced tipping point for the South American monsoon system. *Sci. Rep.* **7**, 1–9 (2017).

22. Feng, X. et al. How deregulation, drought and increasing fire impact Amazonian biodiversity. *Nature* **597**, 516–521 (2021).
23. Ozanne, C. M. et al. Biodiversity meets the atmosphere: a global view of forest canopies. *Science* **301**, 183–186 (2003).
24. Blüthgen, N. et al. How plants shape the ant community in the Amazonian rainforest canopy: the key role of extrafloral nectaries and homopteran honeydew. *Oecologia* **125**, 229–240 (2000).
25. Hölscher, D., Köhler, L., van Dijk, A. I. & Bruijnzeel, L. S. The importance of epiphytes to total rainfall interception by a tropical montane rain forest in Costa Rica. *J. Hydrol.* **292**, 308–322 (2004).
26. Horwath, A. B. et al. Bryophyte stable isotope composition, diversity and biomass define tropical montane cloud forest extent. *Proc. R. Soc. B* **286**, 20182284 (2019).
27. Martinson, G. O. et al. Methane emissions from tank bromeliads in neotropical forests. *Nat. Geosci.* **3**, 766–769 (2010).
28. Obregon, A., Gehrig-Downie, C., Gradstein, S. R., Rollenbeck, R. & Bendix, J. Canopy level fog occurrence in a tropical lowland forest of French Guiana as a prerequisite for high epiphyte diversity. *Agric. For. Meteorol.* **151**, 290–300 (2011).
29. Foster, P. The potential negative impacts of global climate change on tropical montane cloud forests. *Earth-Sci. Rev.* **55**, 73–106 (2001).
30. Morelli, T. L. et al. Climate-change refugia: biodiversity in the slow lane. *Front. Ecol. Environ.* **18**, 228–234 (2020).
31. Gradstein, S. R., Obregon, A., Gehrig, C. & Bendix, J. Tropical lowland cloud forest: a neglected forest type. In *Tropical Montane Cloud Forests* (eds. Bruijnzeel, L. A., Scatena, F. N. & Hamilton, L. S.) 130–133 (Cambridge University Press, 2011). https://doi.org/10.1017/CBO9780511778384.013.
32. Gehrig-Downie, C., Marquardt, J., Obregón, A., Bendix, J., & Gradstein, S. R. Diversity and vertical distribution of filmy ferns as a tool for identifying the novel forest type "tropical lowland cloud forest". *Ecotropica* **18**, 35–44 (2012).
33. Normann, F. et al. Diversity and vertical distribution of epiphytic macrolichens in lowland rain forest and lowland cloud forest of French Guiana. *Ecol. Indic.* **10**, 1111–1118 (2010).
34. Brown, S. C., Wigley, T. M., Otto-Bliesner, B. L., Rahbek, C. & Fordham, D. A. Persistent Quaternary climate refugia are hospices for biodiversity in the Anthropocene. *Nat. Clim. Change* **10**, 244–248 (2020).
35. Ellis, C. J. & Eaton, S. Climate change refugia: Landscape, stand and tree-scale microclimates in epiphyte community composition. *Lichenologist* **53**, 135–148 (2021).
36. Keppel, G. et al. Refugia: identifying and understanding safe havens for biodiversity under climate change. *Glob. Ecol. Biogeogr.* **21**, 393–404 (2012).
37. Tang, C. Q. et al. Identifying long-term stable refugia for relict plant species in East Asia. *Nat. Commun.* **9**, 1–14 (2018).
38. McLaughlin, B. C. et al. Hydrologic refugia, plants, and climate change. *Glob. Change Biol.* **23**, 2941–2961 (2017).
39. Obregon, A., Gehrig-Downie, C., Gradstein, S. R. & Bendix, J. The potential distribution of tropical lowland cloud forest as revealed by a novel MODIS-based fog/low stratus night-time detection scheme. *Remote Sens. Environ.* **155**, 312–324 (2014).
40. Pohl, M. J. et al. A new fog and low stratus retrieval for tropical South America reveals widespread fog in lowland forests. *Remote Sens. Environ.* **264**, 112620 (2021).
41. Gehrig-Downie, C., Obregon, A., Bendix, J. & Gradstein, R. Diversity and vertical distribution of epiphytic liverworts in lowland rain forest and lowland cloud forest of French Guiana. *J. Bryol.* **35**, 243–254 (2013).
42. Klein, V. P., Demarchi, L. O., Quaresma, A. C., da Cruz, J. & Piedade, M. T. F. The vascular epiphyte flora in a white-sand ecosystem of the Uatumã Sustainable Development Reserve. *Central Amazon. Check List* **18**, 157–186 (2022).
43. Singh, J. et al. Enhanced risk of concurrent regional droughts with increased ENSO variability and warming. *Nat. Clim. Change* **12**, 163–170 (2022).
44. Vicente-Serrano, S. M., Beguería, S., López-Moreno, J. I., Angulo, M. & El Kenawy, A. A new global 0.5 gridded dataset (1901–2006) of a multiscalar drought index: comparison with current drought index datasets based on the Palmer Drought Severity Index. *J. Hydrometeorol.* **11**, 1033–1043 (2010).
45. Vicente-Serrano, S. M. et al. Performance of drought indices for ecological, agricultural, and hydrological applications. *Earth Interact.* **16**, 1–27 (2012).
46. Paulo, A. A., Rosa, R. D. & Pereira, L. S. Climate trends and behaviour of drought indices based on precipitation and evapotranspiration in Portugal. *Nat. Hazards Earth Syst. Sci.* **12**, 1481–1491 (2012).
47. Soares-Filho, B. S. et al. Modelling conservation in the Amazon basin. *Nature* **440**, 520–523 (2006).
48. Trachte, K. & Bendix, J. Katabatic flows and their relation to the formation of convective clouds—Idealized case studies. *J. Appl. Meteorol. Climatol.* **51**, 1531–1546 (2012).
49. Trachte, K., Nauss, T. & Bendix, J. The Impact of Different Terrain Configurations on the Formation and Dynamics of Katabatic Flows: Idealised Case Studies. *Bound.-Layer Meteorol.* **134**, 307–325 (2010).
50. Trachte, K., Rollenbeck, R. & Bendix, J. Nocturnal convective cloud formation under clear-sky conditions at the eastern Andes of south Ecuador. *J. Geophys. Res. Atmos.* **115**, D24203 (2010).
51. Baudena, M., Tuinenburg, O. A., Ferdinand, P. A. & Staal, A. Effects of land-use change in the Amazon on precipitation are likely underestimated. *Glob. Change Biol.* **27**, 5580–5587 (2021).
52. Nobre, C. A. et al. Land-use and climate change risks in the Amazon and the need of a novel sustainable development paradigm. *Proc. Natl. Acad. Sci.* **113**, 10759–10768 (2016).
53. Rizzo, R. et al. Land use changes in Southeastern Amazon and trends in rainfall and water yield of the Xingu River during 1976–2015. *Clim. Change* **162**, 1419–1436 (2020).
54. Cox, P. M. et al. Amazonian forest dieback under climate-carbon cycle projections for the 21st century. *Theor. Appl. Climatol.* **78**, 137–156 (2004).
55. Zemp, D. C. et al. Self-amplified Amazon forest loss due to vegetation-atmosphere feedbacks. *Nat. Commun.* **8**, 14681 (2017).
56. Xu, R. et al. Contrasting impacts of forests on cloud cover based on satellite observations. *Nat. Commun.* **13**, 1–12 (2022).
57. Lawrence, D. & Vandecar, K. Effects of tropical deforestation on climate and agriculture. *Nat. Clim. Change* **5**, 27–36 (2015).
58. Arraut, J. M., Nobre, C., Barbosa, H. M. J., Obregon, G. & Marengo, J. Aerial Rivers and Lakes: Looking at Large-Scale Moisture Transport and Its Relation to Amazonia and to Subtropical Rainfall in South America. *J. Clim.* **25**, 543–556 (2012).
59. Weng, W., Luedeke, M. K. B., Zemp, D. C., Lakes, T. & Kropp, J. P. Aerial and surface rivers: downwind impacts on water availability from land use changes in Amazonia. *Hydrol. Earth Syst. Sci.* **22**, 911–927 (2018).
60. Hecht, S. et al. Chapter 14: Amazon in Motion: Changing politics, development strategies, peoples, landscapes, and livelihoods. In *Amazon Assessment Report 2021* (eds. Nobre, C. et al.) (UN Sustainable Development Solutions Network (SDSN), 2021). https://doi.org/10.55161/NHRC6427.
61. Garrett, R. D. et al. Forests and Sustainable Development in the Brazilian Amazon: History, Trends, and Future Prospects. *Annu. Rev. Environ. Resour.* **46**, 625–652 (2021).
62. Barbosa, L. G., Alves, M. A. S. & Grelle, C. E. V. Actions against sustainability: Dismantling of the environmental policies in Brazil. *Land Use Policy* **104**, 105384 (2021).
63. Conceição, K. V. et al. Government policies endanger the indigenous peoples of the Brazilian Amazon. *Land Use Policy* **108**, 105663 (2021).
64. Ruiz Agudelo, C. A. et al. Land use planning in the Amazon basin: challenges from resilience thinking. *Ecol. Soc.* **25**, art8 (2020).
65. Walker, R. T. et al. Avoiding Amazonian catastrophes: Prospects for conservation in the 21st century. *One Earth* **1**, 202–215 (2019).
66. Thom, G. et al. Quaternary climate changes as speciation drivers in the Amazon floodplains. *Sci. Adv.* **6**, eaax4718 (2020).
67. Flecker, A. S. et al. Reducing adverse impacts of Amazon hydropower expansion. *Science* **375**, 753–760 (2022).
68. Nóbrega, R. L. et al. Ecosystem services of a functionally diverse riparian zone in the Amazon–Cerrado agricultural frontier. *Glob. Ecol. Conserv.* **21**, e00819 (2020).
69. Coomes, O. T., Cheng, Y., Takasaki, Y. & Abizaid, C. What drives clearing of old-growth forest over secondary forests in tropical shifting cultivation systems? Evidence from the Peruvian Amazon. *Ecol. Econ.* **189**, 107170 (2021).
70. Villén-Pérez, S., Anaya-Valenzuela, L., Conrado da Cruz, D. & Fearnside, P. M. Mining threatens isolated indigenous peoples in the Brazilian Amazon. *Glob. Environ. Change* **72**, 102398 (2022).
71. Futemma, C., De Castro, F. & Brondizio, E. S. Farmers and Social Innovations in Rural Development: Collaborative Arrangements in Eastern Brazilian Amazon. *Land Use Policy* **99**, 104999 (2020).
72. de Oliveira, G. et al. Protecting Amazonia Should Focus on Protecting Indigenous, Traditional Peoples and Their Territories. *Forests* **13**, 16 (2021).
73. Gehrig-Downie, C., Obregón, A., Bendix, J. & Gradstein, S. R. Epiphyte Biomass and Canopy Microclimate in the Tropical Lowland Cloud Forest of French Guiana: Epiphyte Abundance in Lowland Cloud Forest. *Biotropica* **43**, 591–596 (2011).
74. Tachikawa, T., Hato, M., Kaku, M. & Iwasaki, A. Characteristics of ASTER GDEM version 2. In *2011 IEEE international geoscience and remote sensing symposium* 3657–3660 (IEEE, 2011).
75. Ahlqvist, O. In search of classification that supports the dynamics of science: the FAO Land Cover Classification System and proposed modifications. *Environ. Plan. B Plan. Des.* **35**, 169–186 (2008).
76. Sulla-Menashe, D. & Friedl, M. A. User guide to collection 6 MODIS land cover (MCD12Q1 and MCD12C1) product. *USGS Rest. VA USA* **1**, 18 (2018).
77. Sulla-Menashe, D., Gray, J. M., Abercrombie, S. P. & Friedl, M. A. Hierarchical mapping of annual global land cover 2001 to present: The MODIS Collection 6 Land Cover product. *Remote Sens. Environ.* **222**, 183–194 (2019).
78. Weiss, A. Topographic position and landforms analysis. In *Poster presentation, ESRI user conference*, vol. 200 (San Diego, CA, 2001).

79. Muñoz-Sabater, J. et al. ERA5-Land: A state-of-the-art global reanalysis dataset for land applications. *Earth System Science Data* **13**, 4349–438 (2021).
80. Alam, N. M. et al. Evaluation of drought using SPEI drought class transitions and log-linear models for different agro-ecological regions of India. *Phys. Chem. Earth Parts ABC* **100**, 31–43 (2017).

Acknowledgements

The project was generously funded by the German Research Foundation (Deutsche Forschungsgemeinschaft DFG) under the grants BE 1780/48-1, BA 3843/7-1 and LE 3990/1-1. We thank the German Weather Service (DWD) for providing the KLAM21 model software.

Author contributions

J.B., L.W.L. and M.J.P. designed the research and wrote the paper, M.J.P. performed the analyses. B.T., K.S., M.B.B., S.R.B. and M.Y.B. read and commented on the paper.

Funding

Open Access funding enabled and organized by Projekt DEAL.

Competing interests

The authors declare no competing interests.

Additional information

Supplementary information The online version contains supplementary material available at https://doi.org/10.1038/s43247-023-00867-6.

Correspondence and requests for materials should be addressed to Marius J. Pohl.

Peer review information *Communications Earth & Environment* thanks the anonymous reviewers for their contribution to the peer review of this work. Primary Handling Editors: Min-Hui Lo and Aliénor Lavergne. A peer review file is available